Supporting Information for

Step-wise assembly of a dysprosium-viologen framework with photoswitchable slow magnetic relaxation under zero dc field

Zhen-Na Huang,[a] Lei Zhang,[a] Hao-Ling Sun*[a]

[a] *Department of Chemistry and Beijing Key Laboratory of Energy Conversion and Storage Materials, Beijing Normal University, Beijing 100875, P. R. China. E-mail: haolingsun@bnu.edu.cn*

X-ray crystallography and physical measurement

Intensity data for crystals of **1** and **2** were collected on a rigaku SuperNova, Dual, AtlasS2 diffractometer with graphite-monochromated Cu Kα (λ = 1.5418 Å) or Mo Kα (λ = 0.7107) radiation, respectively. Using Olex2, the structures were solved with the olex2.solve structure solution program using Charge Flipping and refined with the olex2.refine refinement package using Gauss-Newton minimisation. All non-hydrogen atoms were refined anisotropically. Hydrogen atoms were placed at the calculation positions. The details of crystallographic data and selected bond parameters for compounds **1** and **2** are listed in Table S1†, Table S2†, Table S3† and Table S4†, respectively. CCDC 2391044 and 2391045 contain the supplementary crystallographic data for this paper.

The Fourier transform infrared (FT-IR) spectra were recorded using KBr pellets in the range of 4000 to 400 cm^{-1} on an AVATAR 360 Nicolet 380 FT/IR spectrometer. Elemental analyses (C, H, N) were implemented on an Elementar Vario EL analyzer. Powder X-ray diffraction (PXRD) analyses were performed on a Rigaku Dmax-2000 X-ray diffractometer with Cu Kα (λ=1.54059 Å) radiation. Solid-state UV-vis spectra were measured on a TU-1901 spectrophotometer with an integrating sphere at room temperature in the range of 250-850 nm. The UV light was generated by a hand-held UV lamp (365 nm, 100 W). The electron paramagnetic resonance (EPR) spectra were measured using an X-band JEOL FA-200 EPR spectrometer at room temperature. Variable-temperature magnetic susceptibility measurements of **1** and **2** were performed

on Quantum Design PPMS magnetometer (100~10 kHz) and Quantum Design SQUID-MPMS3 (1~1 kHz) magnetometer.

Computational details

Ab initio calculations on the individual Dy^{3+} ion fragment of compound **1** and **2** on the basis of X-ray determined geometry have been carried out with Open MOLCAS program[1] package. The basis sets for all atoms are atomic natural orbitals from the MOLCAS ANO-RCC library: ANO-RCC-VTZP for Dy^{3+} ion; VTZ for close O and N; VDZ for distant atoms. The calculations employed the second order Douglas-Kroll-Hess Hamiltonian, where scalar relativistic contractions were taken into account in the basis set and the spin-orbit coupling were handled separately in the restricted active space state interaction (RASSI-SO) procedure. For the fragment of Dy^{3+} ion, the active electrons in 7 active spaces include all f electrons CAS (9, 7) for Compound **1** and **2** in the CASSCF calculation. To exclude all the doubts, we calculated all the roots in the active space. We have mixed the maximum number of spin-free state which was possible with our hardware (all from 21 sextets, 128 from 224 quadruplets and 130 from 490 doublets for Dy^{3+} ion fragments).

Table S1 Crystallographic Data and Structure Refinement for compounds **1** and **2**.

	1	**2**
Formula	$C_{36}H_{32}DyN_5O_{16}$	$C_{39}H_{35}DyN_5O_{16}$
Mr	953.16	992.22
Crystal system	monoclinic	orthorhombic
Space group	$P2_1/n$	*Pbca*
a (Å)	15.2045(4)	14.4052(6)
b (Å)	14.7944(4)	18.5380(8)
c (Å)	16.1418(4)	29.5150(12)
a (°)	90.00	90.00
β (°)	98.651(2)	90.00
γ (°)	90.00	90.00
V (Å^3)	3589.65(15)	7881.8(6)
Z	4	8
μ (mm^{-1})	11.888	1.978
F (000)	1908.0	3984.0
GOF	1.039	1.062
Data collected	25243	36725
Unique	7156	9624
R_{int}	0.0796	0.0974
*R*1, *wR*2 [$I > 2\sigma(I)$]	0.0531, 0.1355	0.0527, 0.0865
R1, wR2 [all data]	0.0701, 0.1482	0.0973, 0.1064

Table S2 Selected Bond Distances (Å) and Bond Angles (°) in compounds **1** and **2.**

1		**2**	
Dy1-O1	2.273	Dy1-O1	2.269
Dy1-O2	2.319	Dy1-O2	2.261
Dy1-O7W	2.423	Dy1-O7	2.354
Dy1-O3	2.269	Dy1-O3	2.285
Dy1-O4	2.422	Dy1-O4	2.461
Dy1-O5	2.429	Dy1-O5	2.422
Dy1-O6W	2.480	Dy1-O6W	2.418
Dy1-O8W	2.389	Dy1-N1	2.574
O1-Dy1-O2	147.04	O1-Dy1-O2	146.48
O1-Dy1-O7	140.55	O1-Dy1-O7	138.64

Table S3 Hydrogen Bonds in **1**.

D-H	d(D-H) (Å)	<DHA(°)	d(D…A) (Å)	A
O7-H7A	0.85	170.9	2.685	O14
O8-H8A	0.84	141.5	2.747	N4
O8-H8B	0.87	144.9	2.746	O15
O6-H6A	0.88	145.9	2.726	O16
O6-H6B	0.86	158.1	2.782	O11
O10-H10A	0.86	158.9	2.869	O14
O10-H10B	0.86	144.1	2.887	O9
O9-H9B	0.87	173.9	2.896	O5

Table S4 Hydrogen Bonds in **2**.

D-H	d(D-H) (Å)	<DHA(°)	d(D…A) (Å)	A
O6-H6B	0.86	150.1	2.839	O15
O12-H12A	0.85	170.2	2.899	O13
O10-H10B	0.85	159.5	2795	O9
O9-H9A	0.85	169.2	2.773	O15
O9-H9B	0.85	165.4	2.776	O8
O11-H11A	0.85	161.5	2.872	O10
O11-H11B	0.85	154.5	2.889	O14

Table S5 The CShM values calculated by SHAPE 2.0 for **1** and **2**.

Coordination Geometry	**1**	**2**
Octagon (D_{8h})	33.516	30.363
Heptagonal pyramid (C_{7v})	22.752	23.274
Hexagonal bipyramid (D_{6h})	14.496	15.218
Cube (O_h)	12.210	13.233
Square antiprism (D_{4d})	3.375	3.380
Triangular dodecahedron (D_{2d})	1.883	1.728
Biaugmented trigonal prism (C_{2v})	2.541	2.839
Triakis tetrahedron (T_d)	12.765	13.565
Elongated trigonal bipyramid (D_{3h})	24.164	20.417

Table S6 Relaxation fitting parameters from Least-Squares Fitting of $\chi(f)$ data under zero dc field of **2**.

T/K	χ_T	χ_s	α	τ
2	6.671	2.459	0.079	2.64×10^{-4}
2.25	5.965	2.220	0.074	2.61×10^{-4}
2.5	5.398	2.038	0.067	2.57×10^{-4}
2.75	4.931	1.833	0.071	2.47×10^{-4}
3	4.538	1.724	0.063	2.43×10^{-4}
3.25	4.205	1.582	0.066	2.32×10^{-4}
3.5	3.918	1.453	0.068	2.18×10^{-4}
3.75	3.663	1.445	0.045	2.17×10^{-4}
4	3.442	1.341	0.048	2.01×10^{-4}
4.25	3.245	1.316	0.025	1.83×10^{-4}
4.5	3.070	1.216	0.026	1.60×10^{-4}
4.75	2.916	1.124	0.032	1.39×10^{-4}
5	2.776	0.995	0.040	1.17×10^{-4}
5.25	2.645	0.999	0.025	1.01×10^{-4}
5.5	2.536	0.776	0.084	8.66×10^{-5}
5.75	2.398	0.790	0.047	7.48×10^{-5}
6	2.316	0.697	0.070	6.22×10^{-5}
6.25	2.230	0.686	0.069	5.26×10^{-5}
6.5	2.141	0.654	0.056	4.38×10^{-5}
6.75	2.074	0.576	0.090	3.68×10^{-5}
7	1.998	0.579	0.075	3.17×10^{-5}
7.25	1.925	0.587	0.059	2.78×10^{-5}

Table S7 Relaxation fitting parameters from Least-Squares Fitting of $\chi(f)$ data under zero dc field of **2***.

T/K	χ_T	χ_s	α	τ
2	5.944	2.449	0.101	3.03×10^{-4}
2.25	5.337	2.160	0.109	2.97×10^{-4}
2.5	4.832	2.002	0.099	3.01×10^{-4}
2.75	4.413	1.834	0.098	2.98×10^{-4}
3	4.068	1.682	0.102	2.92×10^{-4}
3.25	3.770	1.575	0.097	2.88×10^{-4}
3.5	3.514	1.494	0.090	2.83×10^{-4}
3.75	3.289	1.441	0.076	2.80×10^{-4}
4	3.094	1.309	0.091	2.56×10^{-4}
4.25	2.920	1.163	0.100	2.20×10^{-4}
4.5	2.767	1.090	0.105	1.86×10^{-4}
4.75	2.626	1.045	0.098	1.70×10^{-4}
5	2.792	0.535	0.350	1.45×10^{-4}
5.25	2.620	0.549	0.321	1.20×10^{-4}
5.5	2.509	0.502	0.319	1.00×10^{-4}
5.75	2.353	0.517	0.283	8.54×10^{-5}
6	2.203	0.562	0.228	7.04×10^{-5}
6.25	2.119	0.545	0.224	5.98×10^{-5}
6.5	1.999	0.604	0.164	5.03×10^{-5}
6.75	1.922	0.614	0.146	4.16×10^{-5}
7	1.881	0.581	0.160	3.45×10^{-5}
7.25	1.808	0.583	0.157	2.89×10^{-5}
7.5	1.747	0.609	0.140	2.47×10^{-5}
7.75	1.674	0.591	0.110	2.06×10^{-5}

Table S8 Calculated energy levels (cm^{-1}) and $\boldsymbol{g}$ (g_x, g_y, g_z) tensors of the lowest Kramer doublets (KDs) of the Dy^{3+} fragments, and wavefunction composition for the eight Kramer doublets of the $^6H_{15/2}$ ground multiplet of compounds **1** and **2**.

KDs	**1**			**2**		
	E	***g***	m_J wave functions	*E*	***g***	m_J wave functions
1	0.0	0.246 0.629 19.03	90.8%|±15/2⟩ + 6.0%|±11/2⟩ + 0.8%|±7/2⟩ + 1.2%|±3/2⟩ + 0.7%|±1/2⟩	0.0	0.033 0.069 19.52	95.1%|±15/2⟩ + 2.7%|±11/2⟩ + 0.7%|±9/2⟩ + 1.1%|±7/2⟩ + 0.1%|±5/2⟩
2	25.63	0.215 0.510 18.85	2.2%|±15/2⟩ + 5.4%|±7/2⟩ + 15.6%|±5/2⟩ + 29.0%|±3/2⟩ + 43.7%|±1/2⟩	77.80	0.247 0.318 16.43	82.5%|±13/2⟩ + 3.5%|±11/2⟩ + 10.2%|±9/2⟩ + 1.4%|±7/2⟩ + 2.0%|±5/2⟩
3	142.1	1.138 1.990 13.83	74.0%|±13/2⟩ + 10.7%|±9/2⟩ + 3.2%|±7/2⟩ + 2.9%|±5/2⟩ + 6.7%|±3/2⟩	147.1	2.420 4.743 13.10	37.1%|±11/2⟩ + 8.5%|±9/2⟩ + 17.1%|±7/2⟩ + 15.0%|±5/2⟩ + 9.4%|±1/2⟩
4	197.4	0.443 2.666 14.13	18.7%|±13/2⟩ + 20.3%|±7/2⟩ + 26.5%|±5/2⟩ + 18.7%|±3/2⟩ + 8.1%|±1/2⟩	179.3	8.328 5.761 1.205	31.5%|±11/2⟩ + 12.0%|±7/2⟩ + 7.8%|±5/2⟩ + 25.0%|±3/2⟩ + 13.3%|±1/2⟩
5	263.0	9.564 7.028 1.955	66.1%|±11/2⟩ + 8.1%|±9/2⟩ + 3.8%|±7/2⟩ + 8.6%|±5/2⟩ + 4.1%|±1/2⟩	253.8	7.603 6.579 0.001	6.7%|±13/2⟩ + 36.9%|±9/2⟩ + 20.4%|±5/2⟩ + 4.4%|±3/2⟩ + 26.7%|±1/2⟩
6	295.5	1.464 1.741 12.58	12.0%|±9/2⟩ + 27.8%|±9/2⟩ + 22.0%|±7/2⟩ + 15.6%|±3/2⟩ + 16.6%|±1/2⟩	308.2	2.867 5.137 9.348	11.9%|±11/2⟩ + 10.5%|±9/2⟩ + 23.0%|±7/2⟩ + 28.6%|±3/2⟩ + 23.5%|±1/2⟩
7	313.0	0.702 0.963 14.58	22%|±9/2⟩ + 15.1%|±7/2⟩ + 20.0%|±5/2⟩ + 12.1%|±3/2⟩ + 20.2%|±1/2⟩	354.9	0.730 2.108 15.74	4.6%|±11/2⟩ + 15.0%|±9/2⟩ + 27.7%|±7/2⟩ + 34.2%|±5/2⟩ + 12.9%|±3/2⟩
8	384.5	0.721 1.105 17.41	24.7%|±9/2⟩ + 29.5%|±7/2⟩ + 22.7%|±5/2⟩ + 13.9%|±3/2⟩ + 4.7%|±1/2⟩ +	541.5	0.010 0.013 19.70	11.1%|±9/2⟩ + 16.4%|±7/2⟩ + 19.9%|±5/2⟩ + 22.0%|±3/2⟩ + 23.2%|±1/2⟩

Table S9 *LoProp* charge analysis for the coordination sphere of Dy^{3+} for compounds **1** and **2**.

1		**2**	
O1	-0.855	O1	-0.847
O2	-0.814	O2	-0.812
O7W	-0.752	O7	-0.805
O3	-0.836	O3	-0.822
O4	-0.752	O4	-0.721
O5	-0.757	O5	-0.748
O6W	-0.735	O6W	-0.737
O8W	-0.747	N1	-0.320
$<Axial>_{av}$	-0.807	$<Axial>_{av}$	-0.822
$<Equatorial>_{av}$	-0.765	$<Equatorial>_{av}$	-0.669

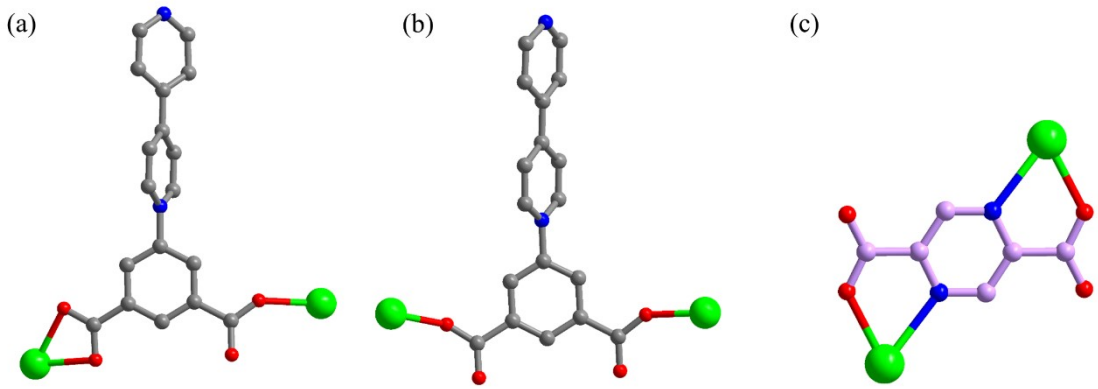

Fig. S1 The coordination modes of ipbp$^-$ ligands in compound **1** (a-b) and the coordination mode of 2,5-pzdc^{2-} bridge in compound **2** (c). The coordination modes of ipbp$^-$ ligands for compound **2** are the same as those of **1**.

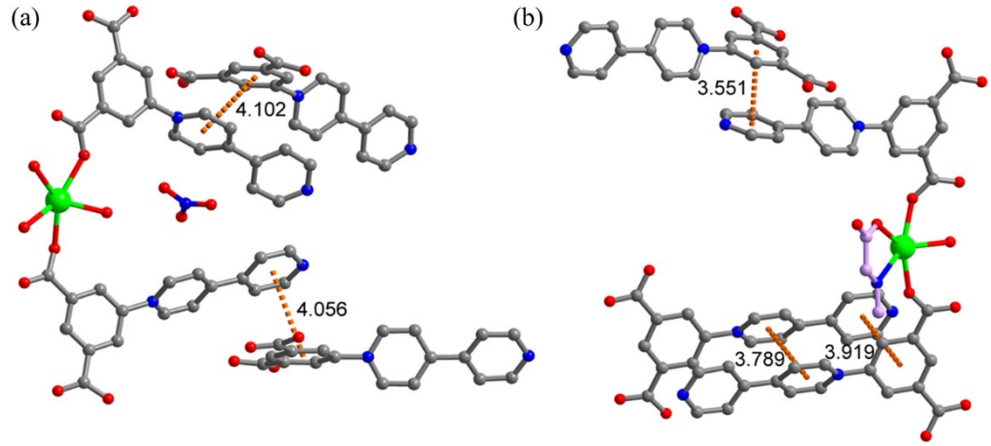

Fig. S2 π-π stacking arrangements (Å) in compound **1** (a) and **2** (b).

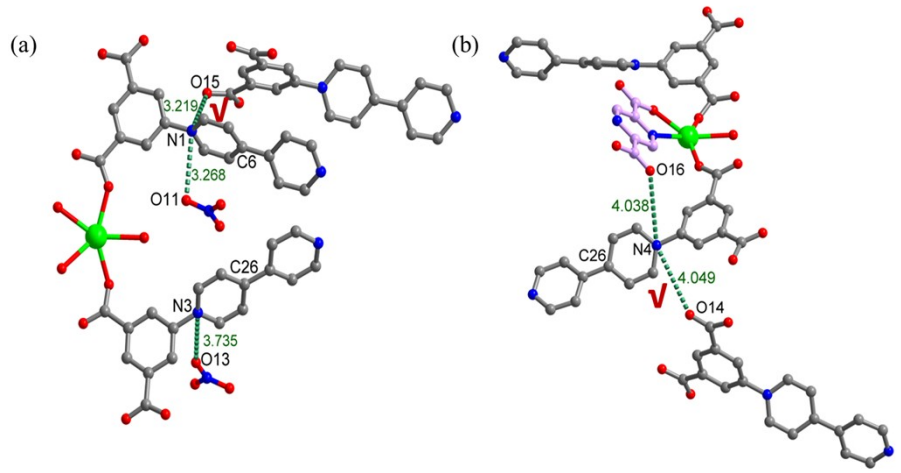

Fig. S3 Donor-acceptor distances (Å) in compounds **1** (a) and **2** (b).

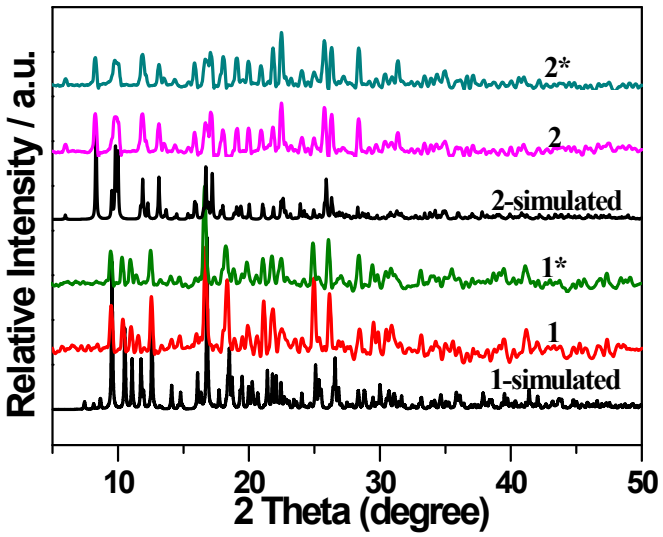

Fig. S4 Powder X-ray diffraction profiles of **1** and **2** before and after irradiation together with simulations from the single crystal data.

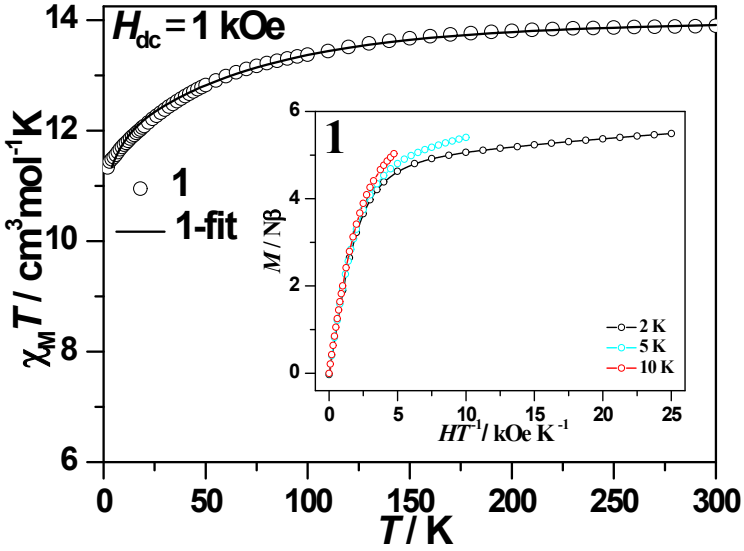

Fig. S5 Temperature-dependent magnetic susceptibilities for **1**, the black line corresponds to the *ab initio* calculation. Inset denotes the plots of *M*-*H* for **1** at 2, 5 and 10 K.

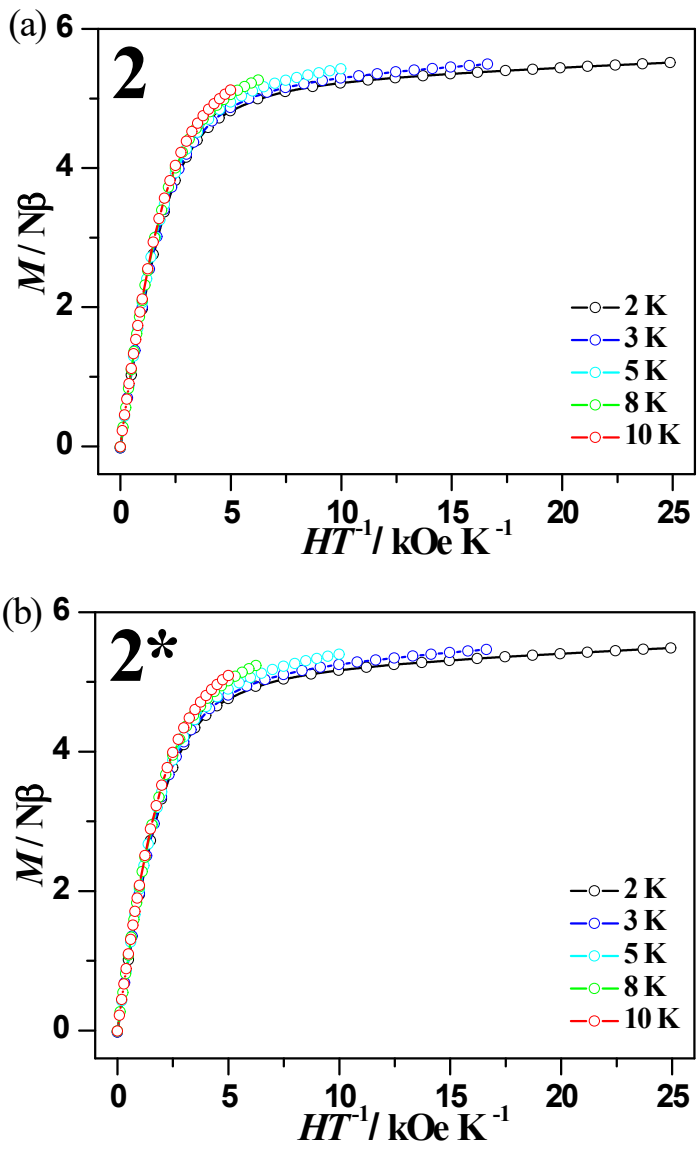

Fig. S6 Plots of *M*-*H* for **2** (a) and **2*** (b) at 2, 3, 5, 8 and 10 K.

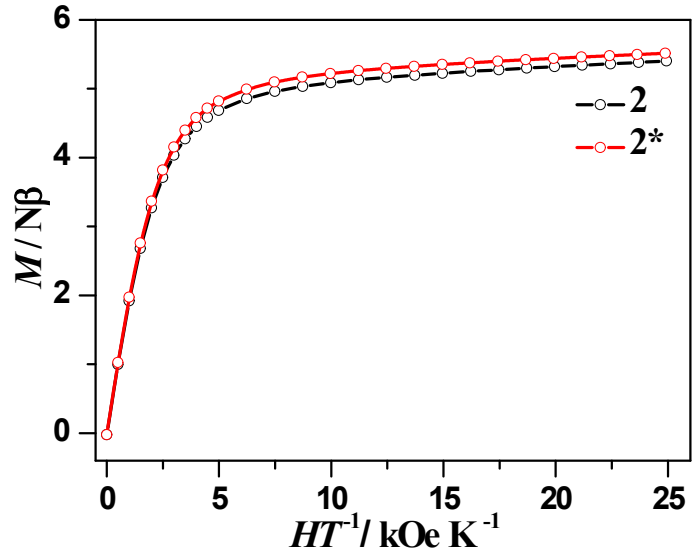

Fig. S7 Plots of *M*-*H* for **2** and **2*** at 2 K.

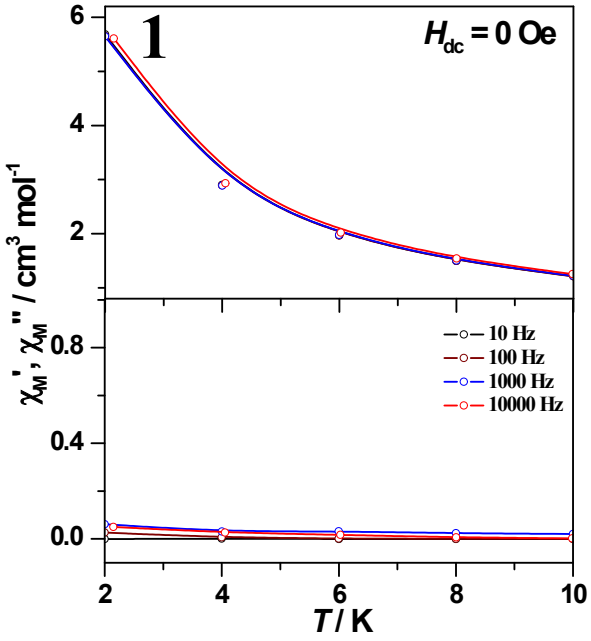

Fig. S8 Temperature-dependent in-phase (χ_M') and out-of phase (χ_M'') ac susceptibility signals under zero dc field for **1**.

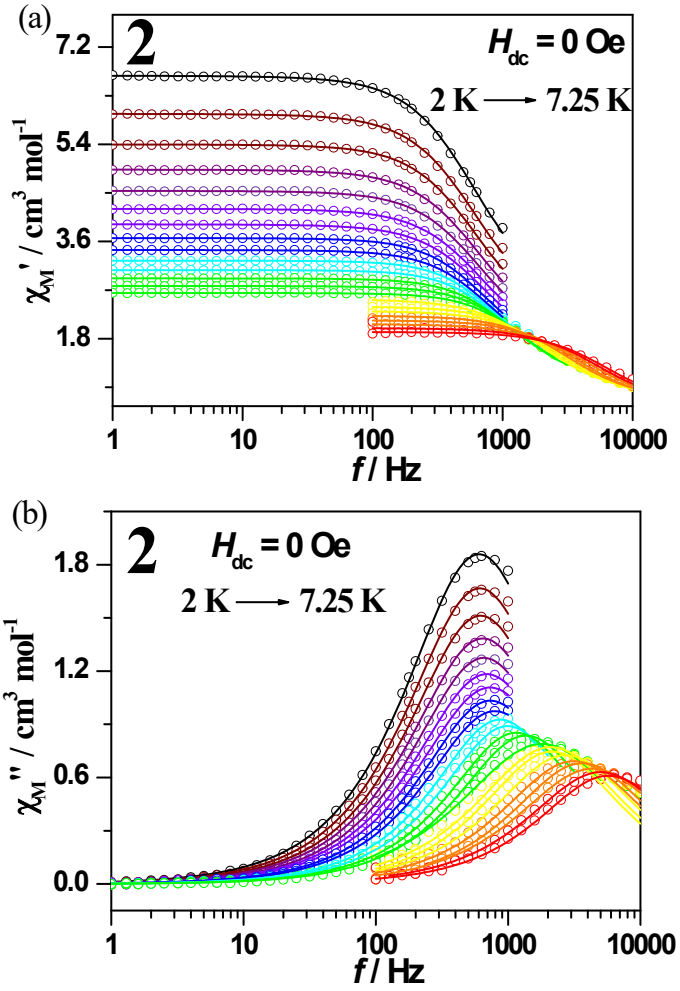

Fig. S9 Ac-f curves measured under zero dc field for **2**. Solid lines were fitted using a generalized Debye relaxation model, simultaneously to χ'(*f*) and χ'' (*f*) curves.

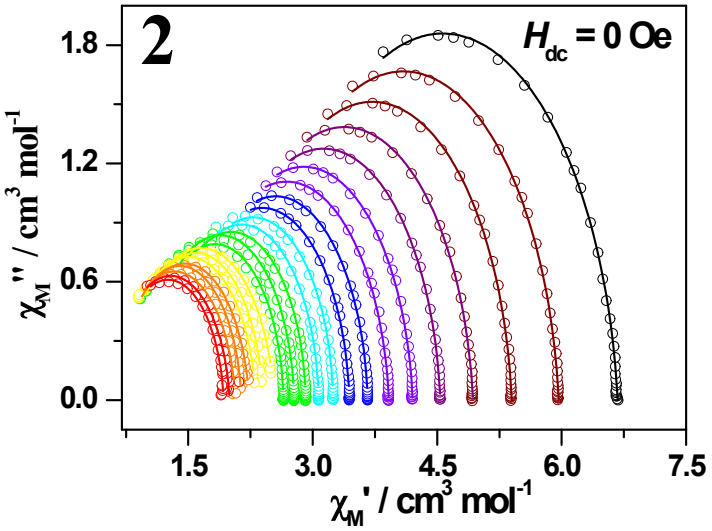

Fig. S10 Cole-cole plots of **2** under zero dc field.

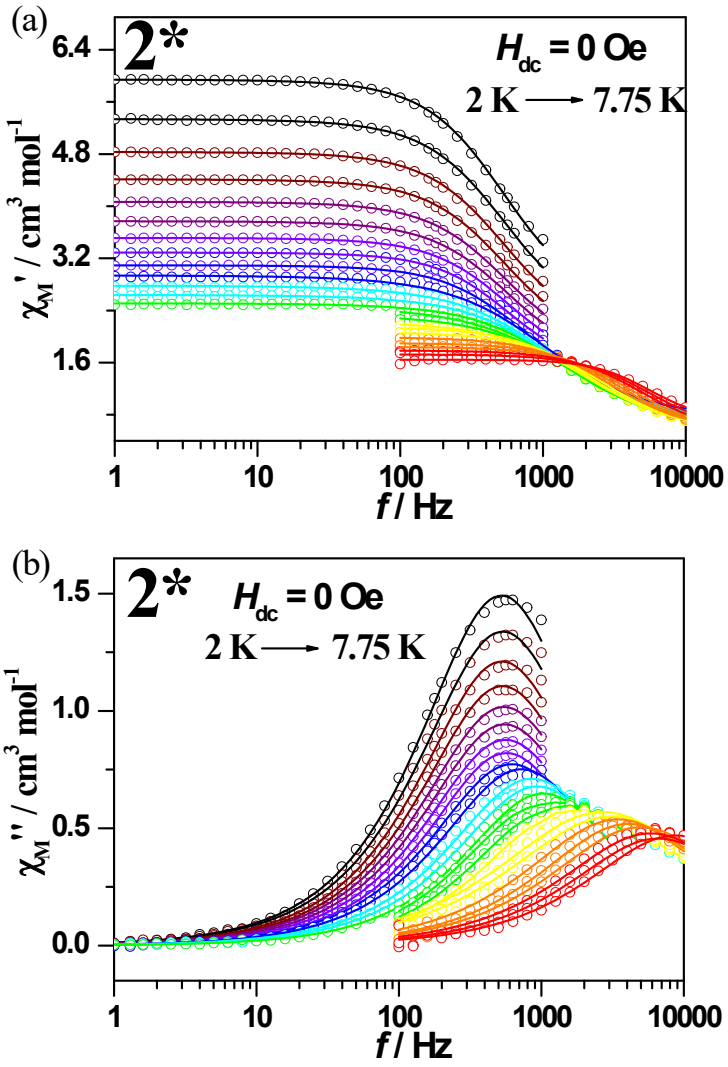

Fig. S11 Ac-f curves measured under zero dc field for **2***. Solid lines were fitted using a generalized Debye relaxation model, simultaneously to χ' (*f*) and χ'' (*f*) curves.

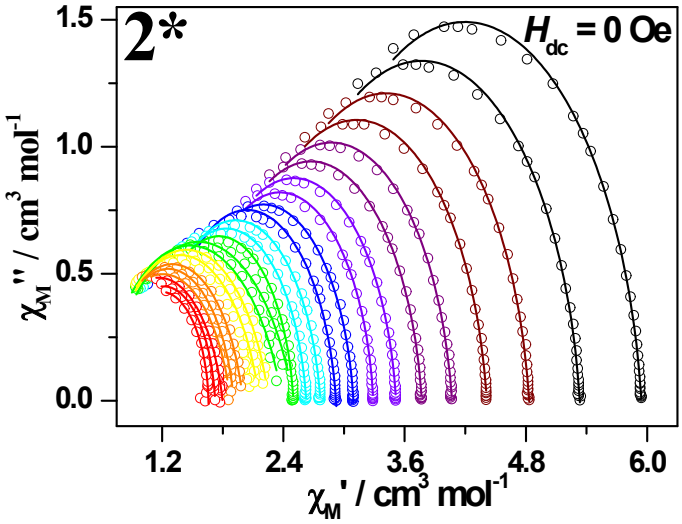

Fig. S12 Cole-cole plots of **2*** under zero dc field.

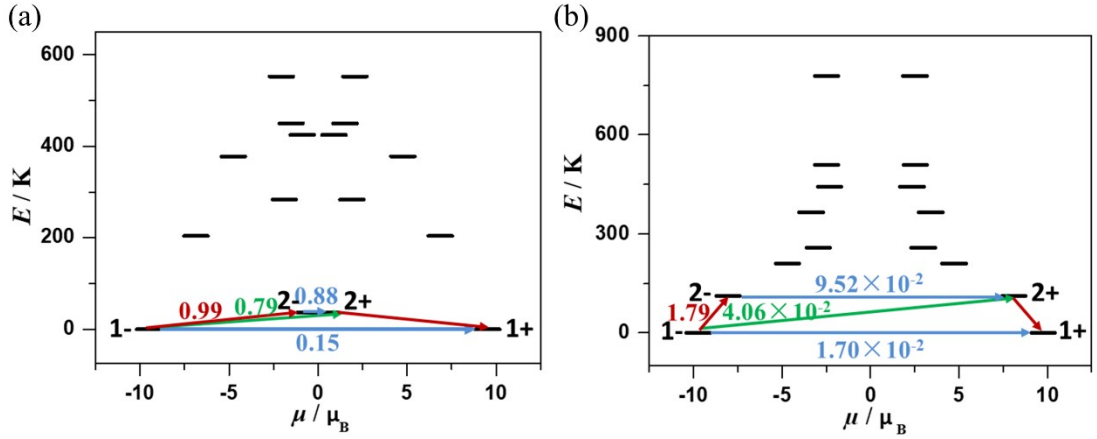

Fig. S13 Magnetization blocking barrier in **1** (a) and **2** (b). The thick black lines denote the Kramers doublets. The numbers at each arrow stand for the mean absolute value of the corresponding matrix element of the transverse moment. The most probable relaxation pathways in compounds **1** and **2** are depicted with red arrows.

REFERENCES

1 (a) G. Karlström, R. Lindh, P.-Å. Malmqvist, B. O. Roos, U. Ryde, V. Veryazov, P.-O. Widmark, M. Cossi, B. Schimmelpfennig, P. Neogrady and L. Seijo, MOLCAS: a program package for computational chemistry, *Comp. Mater. Sci.*, 2003, **28**, 222-239; (b) F. Aquilante, L. De Vico, N. Ferré, G. Ghigo, P. Å. Malmqvist, P. Neogrády, T. B. Pedersen, M. Pitoňák, M. Reiher, B. O. Roos, L. Serrano-Andrés, M. Urban, V. Veryazov and R. Lindh, MOLCAS 7: The Next Generation, *J. Comput. Chem.*, 2009, **31**, 224-247.